CHEMISTRY
A EUROPEAN JOURNAL

DOI: 10.1002/chem.200500411

Synthesis, Crystal Structure, and Catalytic Properties of $MgCo_6Ge_6$

Christine Gieck,[c] Martin Schreyer,[a] Thomas F. Fässler,*[a] Sylwia Cavet,[b] and Peter Claus[b]

Abstract: The ternary compound $MgCo_6Ge_6$ represents a novel member of the RM_6X_6 phases, which contains a graphite-type Ge network, Kagomé nets of Co atoms, and Ge_2 dumbbells with an unexpected short Ge–Ge contact in the range of a localized Ge–Ge single bond. The title compound shows a large variety of chemical bonding, which ranges from metallic to multicenter and covalent bonding. The role of polar intermetallic alloys as promising candidates for the application as catalysts for the selective hydrogenation of α,β-unsaturated aldehydes is discussed. $MgCo_6Ge_6$ possesses a remarkable activity and selectivity for the hydrogenation of *cis*/*trans*-citral to geraniol and nerol.

Keywords: crystal structure · heterogeneous catalysis · host–guest systems · intermetallic compounds · selective hydrogenation

Introduction

While the electronic properties of intermetallic compounds have been studied extensively with respect to stability, electric conductivity, thermoelectric properties, and work functions, their potential as catalysts remains rather unexplored,[1] and only a few attempts have been made to correlate the intrinsic properties of well-defined alloys with their catalytic activity.[2] Up to now no systematic studies on the suitability of intermetallic compounds for catalytic uses have been carried out. There are at least two variables that may have an influence on the catalytic properties of an alloy: 1) the nature of the individual metals and their combination in the alloy, as already known for many examples of bimetallic catalysts, and 2) the structure type and thus the geometric arrangement of the atoms relative to each other. To test the intrinsic properties, catalytic reactions, for example, hydrogenations, have been performed by using the bulk samples instead of supported systems. To enhance the polarity, which is a key factor in controlling the selectivity in the hydrogenation of polar functional groups such as C=O in the presence of an olefinic group,[3] an electropositive metal such as Mg was added in the present study to an equimolar mixture of Ge and Co metal.

In general, the intramolecular selectivity of the hydrogenation of α,β-unsaturated aldehydes, that is, hydrogenation of the C=C group versus the C=O group, can be controlled by the nature of the individual metal, the presence of a second metal (bimetallic catalysts), electron-donating ligand effects by the support material of the catalyst (e.g. through basic zeolites and graphite), steric constraints in the metal environment, strong metal–support interactions (SMSI), selective poisoning, substituents on the C=C bond, solvents, and pressure effects.[3–5] The influence of these parameters can be also found in the selective hydrogenation of citral in numerous studies in the past few years.[6] For example, it has been shown by Singh and Vannice that Pd is the most active metal for citral hydrogenation[6a] and is, in accordance with DFT calculations,[6o] highly selective to C=C bond hydrogenation, yielding citronellal.[6p,q] On the other hand, selectivity towards the allylic alcohols geraniol and nerol was improved by using bimetallic catalysts, for which Sn seems to be the second metal of choice for modifying the base metal as shown, for example, for Rh–Sn catalysts. The formation of alloys, which depends on the type of support material,

[a] Dr. M. Schreyer, Prof. Dr. T. F. Fässler
Department Chemie, Technische Universität München
Lichtenbergstrasse 4, 85748 Garching (Germany)
Fax.:(+49) 89-289-13186
E-mail: thomas.faessler@lrz.tu-muenchen.de

[b] Dipl.-Ing. S. Cavet, Prof. Dr. P. Claus
Ernst-Berl-Institut für Technische und Makromolekulare Chemie
Fachbereich Chemie, TU Darmstadt
Petersenstrasse 20, 64287 Darmstadt (Germany)

[c] Dr. C. Gieck
Present address: Dipartimento di Scienze e Tecnologie Avanzate
Università del Piemonte Orientale
Via Bellini 25/G, 15100 Alessandria (Italy)

catalyst preparation (by an organometallic route or by impregnation), and pretreatment, and their role in controlling the intramolecular selectivity has been a controversial issue. In silica-supported bimetallic Rh–Sn catalysts, an alloy-type phase, in which a tin-enriched phase is preferentially located at the exterior surface of the alloy particles, was reported to be unselective towards the formation of unsaturated alcohols in citral hydrogenation. The preferred activation of the carbonyl group was then attributed to the interaction with SnO_x moieties present in the bimetallic phase formed by surface reconstruction during an induction period.[6m] On the other hand, in studies of citral and crotonaldehyde hydrogenation high selectivities towards unsaturated alcohols were found when bimetallic sites (e.g. $Rh^{\delta-}$–Sn^{δ}, $Ru^{\delta-}$–Fe^{δ}, $Pt^{\delta-}$–Ni^{δ}) of polar character, as indicated by XANES,[7] were present in the alloyed phases.[6l,8a–c] From that it was concluded that surface polarity is a precondition for the adsorption/activation of the C=O group. Furthermore, it has to be noted, that a catalyst comprising an intermetallic compound, Ru_3Sn_7, on an inert oxide support is useful for the selective hydrogenation of carboxylic acids into the corresponding aldehydes.[9]

Here we report the first results of our studies on the catalytic properties of polar intermetallic compounds in the system Mg–Co–Ge, which show that new combinations of elements must be considered to obtain new hydrogenation catalysts. Starting from supported bimetallic Rh–Sn, Ru–Sn, and Pt–Sn catalysts, which are known to catalyze selective hydrogenation reactions,[3] we tested bulk intermetallic compounds in the Co–Sn and Mg–Co–Sn system,[10] and then extended our studies to the Mg–Co–Ge system.

To investigate a series of related compounds, we chose a structure type that allows a variation of both the composition and the components. The structures of ternary intermetallic alloys adopting the RM_6X_6 structure type can be considered as a "filled" variant of the CoSn structure,[11] in which additional interstitial atoms are arranged in one-dimensional tunnels formed by the host framework. Owing to the high flexibility of the host lattice, intercalation products can be obtained for a vast range of guest atoms. $MgCo_6Ge_6$ was first mentioned in 1981 by Schuster et al.,[12] who examined a series of compounds of the RM_6X_6 type (R = Li, Mg, Sc, Y, Zr, Hf, U, or rare-earth metal; M = Fe, Co, Ni, Mn, X = Si, Ge, Sn) in terms of four closely related superstructures of the parent structure type $HfFe_6Ge_6$. In the last two decades, the crystal structures and the magnetic properties of isotypes containing rare-earth metals have been examined.[13] In the case of $HoFe_6Ge_6$,[14] $TbFe_6Sn_6$,[15] and $LiFe_6Ge_6$,[16] superstructures have provided a satisfying description of the average crystal structure. The adopted structure of $DyFe_6Sn_6$ turned out to be dependent on the reaction conditions of its synthesis.[17] High-resolution electron microscopy studies of $HoFe_6Ge_6$[14] indicate the presence of submicroscopically twinned microdomains. Up to now none of the compounds crystallizing in this structure type have been studied with regard to their catalytic properties.

Results and Discussion

Crystal structure: The atomic structure was revealed by single-crystal structure determination. In $MgCo_6Ge_6$, planar graphite-type layers (A) of Ge atoms and Kagomé nets (B) of Co atoms alternate along the *z* axis (crystallographic *c* axis, Figure 1a; Table 1). The resulting columns of vertex-sharing trigonal bipyramids (Figure 1b) form a three-dimensional Co–Ge network with hexagonal tunnels. These tunnels are alternately centered by Mg atoms and Ge_2 dumbbells. There are two different graphite-type layers: one, in which the six-membered rings of Ge1 atoms are centered by Mg atoms ($z = 0$) and a second one ($z(Ge2) = 0.5$), in which the centers of the six-membered rings coincide with the centers of gravity of $(Ge3)_2$ dumbbells, which are also aligned along the *z* axis. The Co–Kagomé nets separate the layers of Ge atoms ($z = 0.2496$). Thus, the crystal structure can be derived from the CoSn structure type[11] by doubling the *c* axis of the parent structure and by alternately replacing interstitial Sn atoms with either one Mg atom or a Ge_2 dumbbell.

The Ge–Ge distance of 2.501 Å for the Ge_2 unit corresponds to values found for Ge–Ge single bonds in various Zintl-type germanides such as $SrGe_2$,[18] $BaGe_2P_2$,[19] and $NaRb_7Ge_8$,[20] whereas the Ge–Ge distances within the graphite-type layers are substantially longer (2.928 Å). The Co–Co distance of 2.536 Å compares to the Co–Co distance in the metal (2.506 Å) and is considerably shorter than related distances in intermetallic compounds containing Co (for example 2.692 Å in $CoSn_3$).

Electronic structure: The LMTO band structure calculations (Figure 2a) reveal individual bands with a large dispersion and a bunch of bands crossing the Fermi level E_F, which is indicative of a metallic behavior (delocalized states). Beside this, several bands run parallel to the energy line at E_F (A-Λ-H-A), which is characteristic for nonbonding and covalent contributions (localized states). As a consequence, the Fermi level lies at a local maximum of the density of states (DOS; Figure 2a). An analysis of the partial contributions to the DOS shows that the states at the Fermi level have predominantly Co character (Figure 2b). The bulk of the germanium contributions is located well below the Fermi level, whereas there are virtually no magnesium contributions at all. This is consistent with the fact that magnesium is the most electropositive element in the compound.

The chemical bonding was further analyzed by means of the electron localization function (ELF). The results of the calculation are given as a three-dimensional (3D) isosurface of constant ELF value in Figure 1c–j. Two-dimensional (2D) intersections are presented as a pixel image, with the density of pixels reflecting the electron density, and the color of each pixel showing the ELF value according to the color bar in Figure 1g, and as a contour line diagram that is superimposed on the pixel image in Figure 1g–m. In the case of an all-electron calculation the shell structure of the core electrons is visible in the 2D images (Figure 1f and 1k–m). For

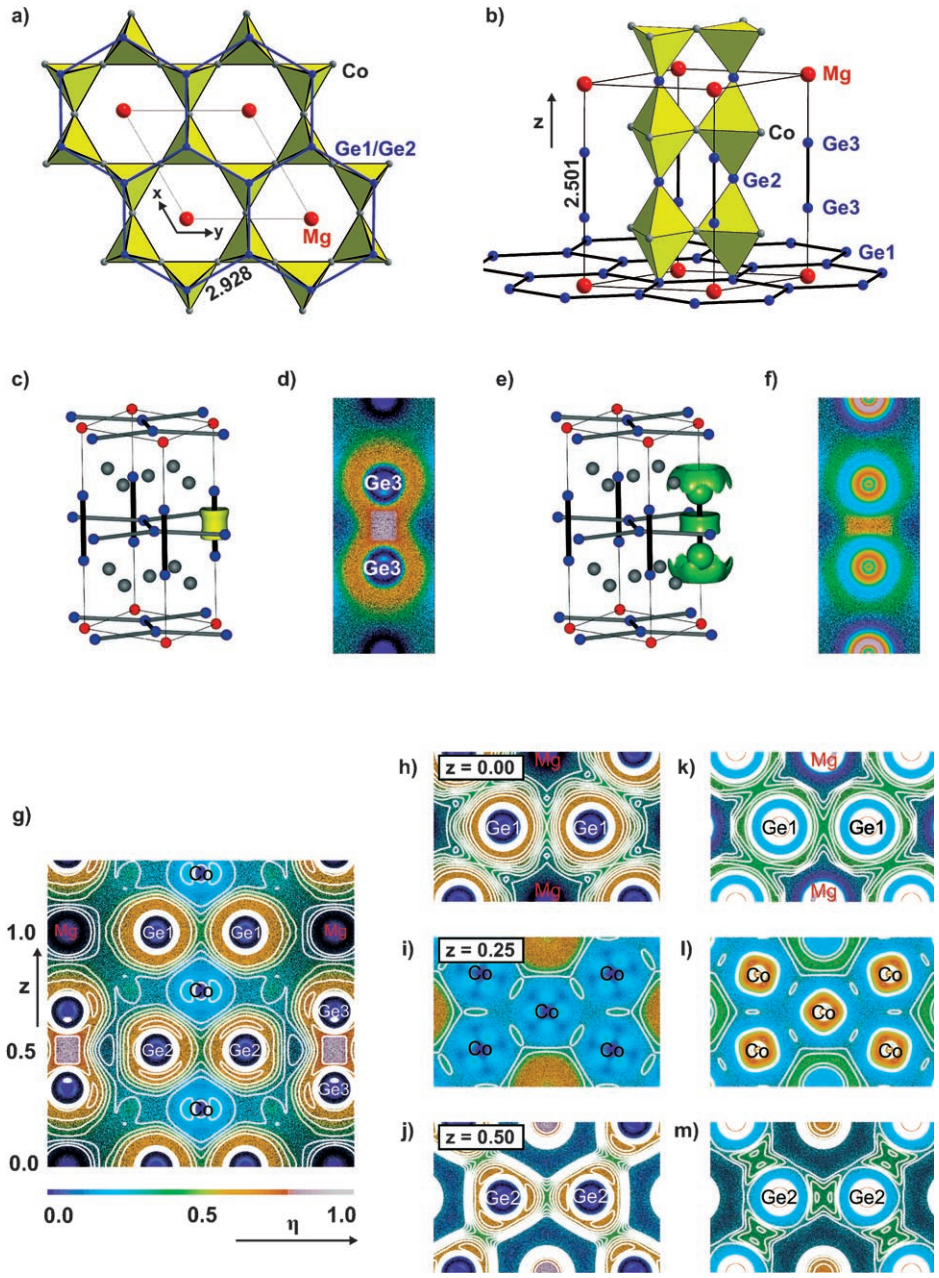

Figure 1. Structure and electronic properties of $MgCo_6Ge_6$. a) View along *c* direction, the graphite-type Ge layers are shown in blue, the Kagomé nets in yellow. b) View perpendicular to *z* axis with special emphasis on the polyhedra formed by the Co atoms of the Kagomé net, the Ge atoms of the graphite net and the Ge_2 dumbbells. c) Valence ELF at the Ge_2 dumbbell 3D isosurface of $\eta = 0.75$. d) Valence ELF at the Ge_2 dumbbell 2D plot. e) Total ELF at the Ge_2 dumbbell 3D isosurface of $\eta = 0.45$. f) Valence ELF at the Ge_2 dumbbell 2D plot. g) Valence ELF along the 110 plane with isobars between 0.3 to 0.7 in steps of 0.1. h) Valence ELF with isobars between 0.3 to 0.65, in steps of 0.05 at $z = 0$. i) Valence ELF with isobars between 0.3 to 0.4, in steps of 0.05 at $z = 0.25$. j) Valence ELF with isobars between 0.3 to 0.65 in steps of 0.05 at $z = 0$. k) Total ELF with isobars between 0.3 to 0.8 in steps of 0.05 at $z = 0$. l) Total ELF with isobars between 0.3 to 0.8 in steps of 0.05 at $z = 0.25$. m) Total ELF with isobars between 0.3 to 0.8 in steps of 0.05 at $z = 0.5$.

Table 1. Bond lengths [Å] for $MgCo_6Ge_6$.

Ge1–Ge1	2.9278(3)	Co1–Co1	2.5354(4)
Ge2–Ge2	2.9278(3)	Mg1–Co1	3.188(1)
Ge3–Ge3	2.501(2)	Co1–Ge1	2.4248(5)
Mg1–Ge1	2.9278(4)	Co1–Ge2	2.4297(5)
Mg1–Ge3	2.622(1)	Co1–Ge3	2.6273(4)

the calculations using only valence electrons, deep blue areas appear at the atom site.

Figure 1c represents a 3D image of the valence electron ELF with a value of $\eta = 0.75$. There is only a region of strongly localized electrons, which has a maximum at the center of the Ge3–Ge3 bond, indicating its covalent character. Figure 1d shows a 2D section of the valence-electron ELF along the Ge3–Ge3 dumbbell in the *bc* plane. The highest maximum of ELF (in white) is found between the two Ge atoms, which are surrounded by an orange area of high electron localization. Figure 1e and 1f show the same section for a total-electron ELF calculation. An ELF isosurface of $\eta = 0.45$ is superimposed in green on the structure (Figure 1e). The 3D representation in the area of the Ge3–Ge3 dumbbell again shows a pronounced maximum between the Ge atoms of the dumbbell. However, in the case of an all-electron calculation the ELF maxima around the Ge atoms opposite the bond become more pronounced. In the 3D picture they are visible in the form of a crown or crest on top of the Ge3 atoms, in the 2D pixel image they appear as deep green areas and can be interpreted as lone pairs at the Ge atoms.

The structural similarity of CoSn and $MgCo_6Ge_6$ also suggests similar electronic properties, in particular strong covalent contributions to the bonding between the germanium atoms within the graphite-like layers, since theoretical investigations by Häußermann et al. showed strong ELF maxima between the tin atoms within the graphite-like layers in CoSn,[21] and no maxima between those tin atoms that fill the hexagonal channels in the Kagomé-type layers. In the case of $MgCo_6Ge_6$ a different situation occurs: The hexagonal channels are filled alternately with Mg atoms and Ge_2

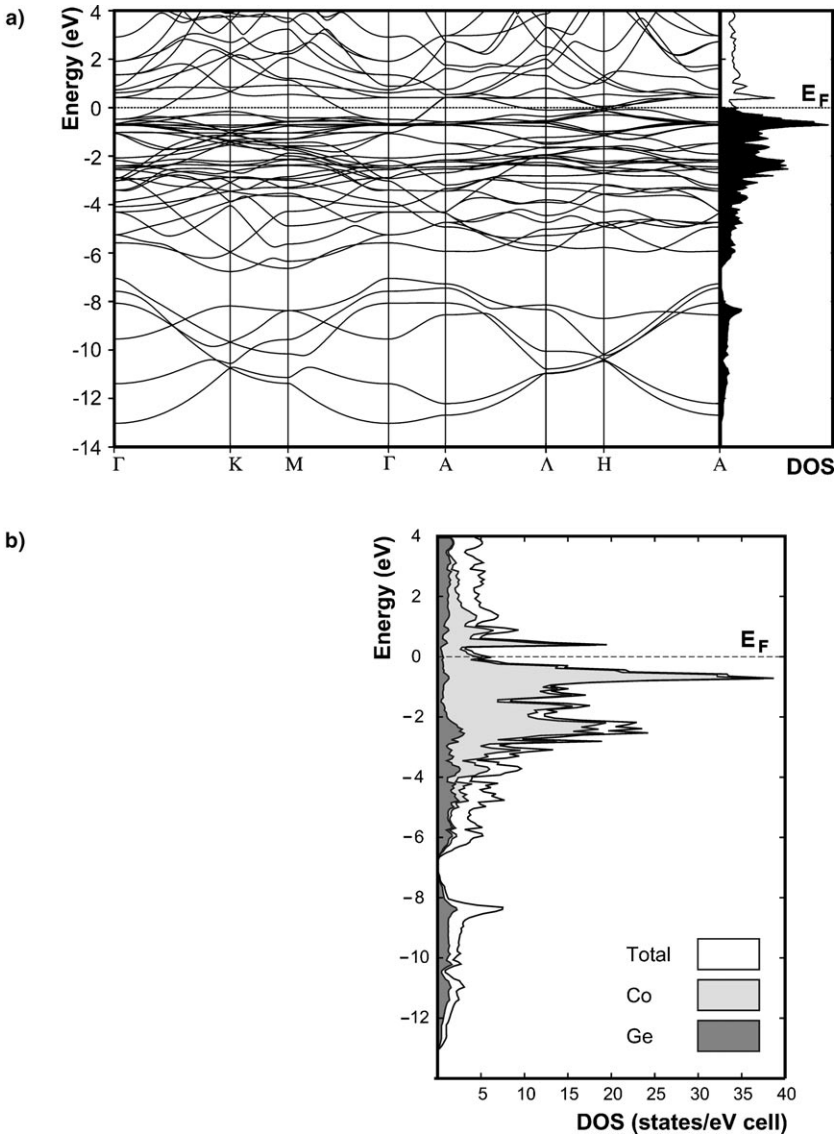

Figure 2. a) Band structure and DOS of $MgCo_6Ge_6$. b) Partial projections of the DOS of $MgCo_6Ge_6$.

dumbbells. Figures 1 g–1 j show a number of two-dimensional cross sections of the valence-electron ELF along defined planes in the structure. Figure 1 g displays a cross section through the unit cell along the 110 plane. The Ge_2 dumbbell is the only pronounced ELF maximum located on an interatomic bond vector in this slice, and there are no maxima between two adjacent Ge1 and two adjacent Ge2 atoms of the two different graphite-like networks. The distance of 2.928 Å between these atoms is considerably longer than that of a covalent Ge–Ge single bond. This is contradictory to the situation in CoSn, in which the shortest homoatomic tin distance is found between the tin atoms of the graphite-like layers and it is much closer in length to a Sn–Sn single bond. This picture is confirmed by several cross sections perpendicular to the *c* axis given in Figure 1 h–m. The Figure 1 h, k, j, m show sections parallel to the graphite-like layers formed by Ge2 and Ge1. Although the ELF maxima between adjacent germanium atoms are oriented towards each other, they are separated by minima. Figure 1 i and l show a similar cut along the 001 plane but in this case through the cobalt atoms of the Kagomé net. Again, the valence ELF is given in Figure 1 h–j, and the total ELF in Figure 1 k–m. Maxima drop off only at very low ELF values ($\eta = 0.2$), indicating a rather small covalent contribution to the bonding between those atoms.

Inspite of some structural similarities between CoSn and $MgCo_6Ge_6$, there are considerable differences in their electronic properties. There is no covalent bonding between the Ge atoms of the graphite layers, whereas the Ge_2 dumbbells in the hexagonal tunnels of the Kagomé-type lattice show a considerable degree of covalent bonding.

Catalytic activity: The hydrogenation of citral (3,7-dimethyl-2,6-octadienal) was chosen as a test reaction. Citral has three unsaturated bonds including conjugated C=C and C=O groups as well as an isolated C=C bond. Selective hydrogenation of this α,β-unsaturated aldehyde leads to industrially important compounds, for example, for the perfumery and flavoring industry. In particular, citronellal is formed by hydrogenation of the olefinic group which is conjugated to the C=O group, whereas hydrogenation of the latter yields unsaturated *trans* and *cis* alcohols (geraniol and nerol, respectively). Under certain reaction conditions and depending on the catalyst type, consecutive hydrogenation of these intermediates can occur leading to citronellol, dihydrocitronellal, and 3,7-dimethyloctanol.

Whereas binary Co–Ge alloys show only a low citral conversion (3% at 448 K, 8 MPa), which is obviously independent of the Co/Ge ratio,[22] the catalytic activity is strongly increased by the introduction of Mg. For $MgCo_6Ge_6$ samples, a citral conversion of 17% was obtained at a reaction temperature of 448 K, which is considerably higher than the 3% achieved with binary Co–Ge alloys. Furthermore, the catalyst shows an increased selectivity to give geraniol and nerol in almost 50% (Table 2), instead of the 3–10% obtained by using the binary alloys. For comparison, Table 2 also con-

Table 2. Catalytic results of citral hydrogenation over $MgCo_6Ge_6$ and a supported reference catalyst (Ru-Sn/SiO_2) at 448 K.

	$MgCo_6Ge_6$[a]	Ru–Sn/SiO_2[b]
citral conversion [%]	17.1	48.2
activity [mol/g_{cat} h]	0.004	0.072
selectivity [%]		
geraniol + nerol[c]	48.3	72.4
citronellal[d]	5.2	9.3
citronellol[e]	5.2	8.5
other products[f]	41.3	9.8
geraniol/nerol	2.1	1.6
(geraniol + nerol)/(citronellal + citronellol)	4.6	4.1

[a] $m_{cat}=100$ mg, $c^0_{citral}=0.58$ mol L^{-1}, $p_{H_2}=7.5$ MPa, $t=150$ min. [b] $m_{cat}=465$ mg, $c^0_{citral}=1.11$ mol L^{-1}, $p_{H_2}=8.5$ MPa, $t=100$ min, 300-mL Parr batch reactor. The Ru–Sn/SiO_2 catalyst was prepared according to CSR (controlled surface reaction) method.[3] [c] (*trans* + *cis*) Product of C=O group hydrogenation. [d] Product of conjugated C=C bond hydrogenation. [e] Product of consecutive hydrogenation of geraniol, nerol, and citronellal. [f] Isopulegol, menthol, and non-identified products.

tains the catalytic properties of a supported bimetallic reference catalyst (Ru–Sn/SiO_2) which is commonly used for the synthesis of higher unsaturated alcohols. Although the activity of $MgCo_6Ge_6$ is one order of magnitude lower than the reference catalyst, which contains the active components in the form of bimetallic nanoparticles in high dispersion on an oxidic support, the most striking property of the polar intermetallic title compound is the formation of the desired unsaturated alcohols at comparable levels as indicated, for example, by the product ratio of (geraniol + nerol)/(citronellal + citronellol). The results obtained for $MgCo_6Ge_6$ clearly indicate that the modification of the binary Co–Ge alloy by introducing the electropositive metal Mg increases the polarity which, according to the proposed reaction mechanism,[3] is a prerequisite for the chemisorption of the polar C=O group through the oxygen atom and, thus, for controlling the intramolecular selectivity towards unsaturated alcohols.

It should be noted that the catalytic activity and selectivity is highly dependent of the sample preparation. In view of the fact that we cannot exclude that $MgCo_6Ge_6$ samples contain also amorphous materials beside unreacted Ge, the catalytic properties may not only result from the intrinsic properties of the novel phase $MgCo_6Ge_6$. However, since we tested various binary products with lower conversion rates, the introduction of the more electropositive component must play a crucial role in enhancing the catalytic properties.

Conclusion

The present study shows that a combination of elements of different electronegativity in the form of a polar intermetallic compound possesses catalytic activity, even though none of the constituting elements does so. Thus, the investigation of ternary alloys of various compositions might enable the substitution of some rather expensive one- or two-component metal catalysts by cheaper three- or more-component ones.

Experimental Section

Preparation: $MgCo_6Ge_6$ was synthesized by arc melting of the elements followed by subsequent annealing of the reaction product. A mixture of magnesium (Alfa Aesar, 99.8%), cobalt (Chempur, 99.9%), and germanium (Aldrich, 99.999%) in the molar ratio 1:2:3 was fused under an argon atmosphere in the reaction chamber of an arc melter (Johanna Otto GmbH, MAM-1), and the regulus was annealed in a programmable tube furnace at 650 °C for 12 h. The product consisted of xenomorphous crystals with a metallic luster. The purity of the sample was checked by using a STOE STADI P powder diffractometer with a $Cu_{K\alpha}$ source. The powder diffractogram, which could be indexed by using the theoretical powder pattern calculated from the single-crystal data of $MgCo_6Ge_6$,[23] showed that a nearly single-phase product with small amounts of unreacted Ge was obtained. The crystallinity of the samples was highly dependent on the conditions of the arc-melt process and could be increased by subsequent thermal treatment. Variations of the conditions of the arc-melting process also yield a novel phase, which was subsequently characterized as $MgCo_4Ge_6$. Other reactions starting from the same Mg:Co:Ge ratio of 2:3:4 showed the formation of mixtures containing $MgCo_4Ge_6$, $MgCo_6Ge_6$, $CoGe_2$, and Ge. In all cases a mass loss is observed, which mainly originates from the loss of magnesia during the arc-melting process.

In the case of binary samples various ratios of Co and Ge were loaded in an arc-melting furnace and heated repeatedly. The resulting products consist of CoGe and $CoGe_2$ together with unreacted Ge.

Crystal structure determination: The structure of $MgCo_6Ge_6$ was determined from single-crystal X-ray diffraction data. A single crystal was selected from the reaction mixture and placed into an oil-filled glass capillary. The measurement was performed on an Oxford Diffraction Xcalibur 3 diffractometer equipped with a monochromatic $Mo_{K\alpha}$ source ($\lambda=0.71073$ Å). The exposure time was 80 s per frame. The collection of intensity data was carried out with the CrysAlis program.[24] The final lattice parameters were calculated from all reflections observed in the actual data collection. A summary of the experimental and crystallographic data is given in Table 3.

The structure was solved by direct methods, which revealed the atomic positions, and refined by using the SHELX-97 program package.[25] The final refinements were carried out on F_O^2. Atomic scattering factors for spherical neutral free atoms were taken from standard sources, and anomalous dispersion corrections were applied.[26] Calculations performed at an intermediate stage in which the relative positional occupancies of the interstitial atoms were refined, did not indicate any non-stoichiometry of the compound. The final coordinates and equivalent isotropic temperature factors of all atoms are given in Table 4.

Quantum-chemical calculations: The electronic structure was investigated by means of the ab initio full-potential linear muffin-tin orbital (LMTO) method in the atomic sphere approximation (ASA), using the tight-binding (TB) program TB-LMTO-ASA.[27] The calculations were based on the local-density approximation (LDA), and the Hedin–Lundquist parameterization was employed for exchange and correlation potentials.[28] The radii of the muffin-tin spheres and empty spheres were determined according to Jepsen and Andersen.[29] For the calculations s, p, and "down-folded" d partial waves for Ge, s, p, and "down-folded" d partial waves for Mg, and s, p and d partial waves for Co were used.

A topographical analysis of the electron density distribution using the electron localization function (ELF), which originally was introduced for the deduction of the shell structure of atoms from the electron density,[30] gives further insight into the chemical bonding in intermetallic compounds. ELF values are scaled between 0 and 1, with high ELF values and local ELF maxima corresponding to areas and centers of localized electrons, and low ELF values defining the spatial area around these maxima. The resulting partition of space into areas of high electron local-

Table 3. Crystal data and structure refinement for $MgCo_6Ge_6$.[a]

empirical formula	$MgCo_6Ge_6$
formula weight	813.43
temperature [K]	293(2)
wavelength [Å]	0.71073
crystal system	hexagonal
space group	*P6/mmm*
unit cell dimensions	
a [Å]	5.0709(7)
c [Å]	7.745(2)
volume [Å^3]	172.46(5)
Z	1
ρ_{calcd} [g cm^{-3}]	7.832
μ [mm^{-1}]	39.721
F(000)	366
crystal size [mm^3]	$0.1\times0.15\times0.2$
theta range for data collection	4.64 to 39.69°
index ranges	$-8\le h\le7$, $-7\le k\le9$, $-12\le l\le13$
reflections collected	2787
independent reflections	248
completeness to $\theta=27.54°$	96.1 %
absorption correction	CrysAlis[13]
refinement method	full-matrix least-squares on F^2
data/restraints/parameters	248/0/15
goodness-of-fit on F^2	1.280
final R indices *[I>2σ(I)]*	$R_1=0.027$, $wR_2=0.086$
R indices (all data)	$R_1=0.029$, $wR_2=0.087$
largest diff. peak and hole [e Å^{-3}]	2.471 and −2.076

[a] Further details of the crystal structure investigation may be obtained from the Fachinformationszentrum Karlsruhe, 76344 Eggenstein-Leopoldshafen, Germany (fax: (+49) 7247-808-666; e-mail: crysdata@fiz-karlsruhe.de) on quoting the depository number CSD-415256.

Table 4. Atomic coordinates and equivalent isotropic displacement parameters (Å$^2\times10^3$) for $MgCo_6Ge_6$. *U(eq)* is defined as one third of the trace of the orthogonalized U_{ij} tensor.

	x	*y*	*z*	*U(eq)*
Mg1	0	0	0	21(1)
Co1	0	0.5000	0.2496(1)	16(1)
Ge1	0.3333	0.6667	0	12(1)
Ge2	0.3333	0.6667	0.5000	11(1)
Ge3	0	0	0.3385(1)	13(1)

ization can be interpreted in terms of bonding and nonbonding electron pairs and reveals their three-dimensional shape. Thus, spatial domains of localized electrons become visible.[31–34] These calculations can be carried out either with valence electrons only, or by including all electrons for the ELF analysis.

Catalytic activity of $MgCo_6Ge_6$: A high-pressure batch reactor[35] was filled with a solution of citral (1 mL; 47 % *cis*-citral, 53 % *trans*-citral) in hexane (9 mL). After the addition of powdered $MgCo_6Ge_6$ (100 mg with small amounts of unreacted Ge), the reactor was flushed with argon and heated to 448 K. The hydrogen pressure in the batch reactor was set to 7.5 MPa, and the reaction mixture was stirred at 850 rpm for 150 min. The composition of the product was determined by GC analysis (HP 5890, flame ionization detector, DB-WAX capillary column).

Acknowledgements

This work was supported by the Deutsche Forschungsgemeinschaft (project number FA 198/4–1 and CL 168/3–1: Polare Legierungen als Mehrkomponenten-Katalysatoren). We thank Dr. A. Schier for the revision of the manuscript and R. Klemens for the synthesis of some of the alloys.

[1] *Catalysis from A to Z* (Eds.: B. Cornils, W. A. Herrmann, R. Schlögl, C-H. Wong) Wiley-VCH, Weinheim **2000**.
[2] a) G. C. Bond, *Catalysis by Metals*, Academic Press, New York, **1962**. b) Poster abstract at *12th Conference of GDCh Division of Solid State Chemistry and Material Research*, Marburg (Germany), **2004**, C. Gieck, T. F. Fässler, S. Cavet, P. Claus, *Z. Anorg. Allg. Chem.* **2004**, *630*, 1724.
[3] P. Claus, *Top. Catal.* **1998**, *5*, 51.
[4] M. Bron, D. Teschner, A. Knop-Gericke, A. Scheybal, B. Steinhauer, M. Hävecker, R. Födisch, D. Hönicke, R. Schlögl, P. Claus, *Catal. Commun.* **2005**, *6*, 371.
[5] P. Gallezot, D. Richard, *Catal. Rev. Sci. Eng.* **1998**, *40*, 81.
[6] a) U. K. Singh, M. A. Vannice, *J. Catal.* **2001**, *199*, 73; b) U. K. Singh, M. N. Sysak, M. A. Vannice, *J. Catal.* **2000**, *191*, 181; c) U. K. Singh, M. A. Vannice, *J. Catal.* **2000**, *191*, 165; d) U. K. Singh, M. A. Vannice, *J. Mol. Catal. B J. Mol. Catal. A* **2000**, *163*, 233; e) S. Galvagno, C. Milone, G. Neri, A. Donato, R. Pietropaolo, *Stud. Surf. Sci. Catal.* **1993**, *78*, 163; f) C. Milone, M. L. Tropeano, G. Gulino, G. Neri, R. Ingoglia, S. Galvagno, *Chem. Commun.* **2002**, 868; g) R. Malathi, R. P. Viswanath, *Appl. Catal. A* **2001**, *208*, 323; h) B. Didillon, J. P. Candy, A. Elmansour, C. Houtmann, J. M. Basset, *J. Mol. Catal.* **1992**, *74*, 43; i) S. Galvagno, C. Milone, A. Donato, G. Neri, R. Pietropaolo, *Catal. Lett.* **1993**, *17*, 55; j) G. Neri, L. Mercadante, C. Milone, R. Pietropaolo, S. Galvagno, *J. Mol. Catal. A* **1996**, *108* , 41; k) P. Reyes, H. Rojas, G. Pecchi, J. L. G. Fierro, *J. Mol. Catal. A* **2002**, *179*, 293; l) B. Bachiller-Baeza, A. Guerrero-Ruiz, P. Wang, I. Rodriguez-Ramos, *J. Catal.* **2001**, *204* , 450; m) L. Sordelli, R. Psaro, G. Vlaic, A. Cepparo, S. Recchia, C. Dossi, A. Fusi, R. Zanoni, *J. Catal.* **1999**, *182*, 186; n) S. Recchia, C. Dossi, A. Fusi, L. Sordelli, R. Psaro, *Appl. Catal. A* **1999**, *182*, 41; o) F. Delbecq, P. Sautet, *J. Catal.* **1995**, *152*, 217; p) M. A. Aramendia, V. Borau, C. Jimenez, J. M. Marinas, A. Porras, F. J. Urbano, *J. Catal.* **1997**, *172*, 46; q) J. Aumo, J. Lilja, P. Maki-Arvela, T. Salmi, M. Sundell, H. Vainio, D. Y. Murzin, *Catal. Lett.* **2002**, *84*, 219; r) J. N. Coupé, E. Jordao, M. A. Fraga, M. J. Mendes, *Appl. Catal. A* **2000**, *199*, 45.
[7] A. Jentys, B. J. McHugh, G. L. Haller, J. A. Lercher, *J. Phys. Chem.* **1992**, *96*, 1324.
[8] a) P. Claus, *Chem. Ing. Tech.* **1995**, *67*, 1340; b) H. Berndt, H. Mehner, P. Claus, *Chem. Ing. Tech.* **1995**, *67*, 1332; c) C. G. Raab, M. Englisch, T. B. L. W. Marinelli, J. A. Lercher, *Stud. Surf. Sci. Catal.* **1993**, *78*, 211.
[9] R. Jacquot, J.-M. Leclercq, C. Mercier, J.-M. Popa, WO9622832, 01 August 1995, appl. to Rhone-Poulenc Chimie.
[10] a) M. Schreyer, G. Kraus, T. F. Fässler, *Z. Anorg. Allg. Chem.* **2004**, *630*, 2520; b) M. Schreyer, G. Kraus, T. F. Fässler, poster abstract at *9th European Conference of Solid State Chemistry*, P078, Stuttgart, **2003**; c) M. Schreyer, S. Cavet, P. Claus, T. F. Fässler, poster abstract at the annual meeting of GDCh, FKM-KAT-002, Munich, **2003**.
[11] O. Nial, *Z. Anorg. Allg. Chem.* **1938**, *238*, 287.
[12] W. Buchholz, H.-U. Schuster, *Z. Anorg. Allg. Chem.* **1981**, *482*, 40.
[13] G. Venturini, R. Welter, B. Malaman, *J. Alloys Compd.* **1992**, *185*, 99.
[14] O. Oleksyn, H.-U. Nissen, R. Wessicken, *Phil. Mag. Letters* **1998**, *77*, 275.
[15] P. Schobinger-Papamantellos, O. Oleksyn, J. Rodríguez-Carvajal, K. H. J. Buschow, *J. Magn. Magn. Mater.* **1998**,*182*, 96.
[16] E. Welk, H.-U. Schuster, *Z. Anorg. Allg. Chem.* **1976**, *424*, 193.
[17] O. Oleksyn, H. Böhm, *Z. Kristallogr.* **1998**, *213*, 270.
[18] J. Evers, G. Oehlinger, A. Weiss, *Z. Naturforsch. B* **1979**, *34*, 524.
[19] B. Eisenmann, H. Schäfer, *Z. Naturforsch. B* **1981**, *36*, 415.

[20] J. Llanos, R. Nesper, H. G. von Schnering, *Angew. Chem.* **1983**, *95*, 1026; *Angew. Chem. Int. Ed. Engl.* **1983**, *22*, 998.
[21] S. I. Simak, U. Häußermann, I. A. Abrikosov, O. Eriksson, J. M. Wills, S. Lidin, B. Johansson, *Phys. Rev. Lett.* **1997**, *79*, 1333.
[22] Various mixtures with Co and Ge powders were heated by arc melting. The amorphous products were tested for catalytic behaviour.
[23] W. Kraus, G. Nolze, *J. Appl. Crystallogr.* **1996**, *29*, 301.
[24] Oxford Diffraction, 2003, Oxford Diffraction Ltd., Xcalibur CCD system, CrysAlis Software system, Version 1.170.
[25] G. M. Sheldrick, SHELXL-97: Program for crystal structure refinement, University of Göttingen, **1997**.
[26] D. T. Cromer, J. T. Waber, *International Tables for X-Ray Crystallography*, Kynoch Press, Birmingham, England, **1974**, Vol. IV, Table 2.2 A and Table 2.3.1.
[27] M. van Schilfgarde,T. A. Paxton, O. Jepsen, O. K. Andersen, G. Krier, Programm TB-LMTO; Max-Planck-Institut für Festkörperforschung: Stuttgart, **1994**.
[28] U. Barth, L. Hedin, *J. Phys. Chem.* **1972**, *76*, 1629.
[29] O. Jepsen, O. K. Andersen, *Z. Phys. B* **1995**, *97*, 35.
[30] A. D. Becke, E. J. Edgecombe, *Chem. Phys.* **1990**, *92*, 5397.
[31] A. Savin, A. D. Becke, J. Flad, R. Nesper, H. G. von Schnering, *Angew. Chem.* **1991**, *103*, 421; *Angew. Chem. Int. Ed. Engl.* **1991**, *30*, 409.
[32] B. Silvi, A. Savin, *Nature* **1994**, *371*, 683.
[33] A. Savin, R. Nesper, S. Wengert, T. F. Fässler, *Angew. Chem.* **1997**, *36*, 1892; *Angew. Chem. Int. Ed. Engl.* **1997**, *36*, 1809.
[34] R. F. W. Bader, *Coord. Chem. Rev.* **2000**, *197*, 71.
[35] M. Lucas, P. Claus, *Chem. Ing. Tech.* **2001**, *73*, 252.

Received: April 12, 2005
Revised: September 21, 2005
Published online: December 19, 2005

